Soft Matter

PAPER

View Article Online
View Journal

Cite this: DOI: 10.1039/c6sm01445c

A mathematical model for electrical impedance spectroscopy of zwitterionic hydrogels

Sarah E. Feicht and Aditya S. Khair*

Received 22nd June 2016,
Accepted 22nd July 2016

DOI: 10.1039/c6sm01445c

www.rsc.org/softmatter

We report a mathematical model for ion transport and electrical impedance in zwitterionic hydrogels, which possess acidic and basic functional groups that carry a net charge at a pH not equal to the isoelectric point. Such hydrogels can act as an electro-mechanical interface between a relatively hard biosensor and soft tissue in the body. For this application, the electrical impedance of the hydrogel must be characterized to ensure that ion transport to the biosensor is not significantly hindered. The electrical impedance is the ratio of the applied voltage to the measured current. We consider a simple model system, wherein an oscillating voltage is applied across a hydrogel immersed in electrolyte and sandwiched between parallel, blocking electrodes. We employ the Poisson–Nernst–Planck (PNP) equations coupled with acid–base dissociation reactions for the charge on the hydrogel backbone to model the ionic transport across the hydrogel. The electrical impedance is calculated from the numerical solution to the PNP equations and subsequently analyzed *via* an equivalent circuit model to extract the hydrogel capacitance, resistance, and the capacitance of electrical double layers at the electrode–hydrogel interface. For example, we predict that an increase in pH from the isoelectric point, pH = 6.4 for a model PCBMA hydrogel, to pH = 8 reduces the resistance of the hydrogel by ~40% and increases the double layer capacitance by ~250% at an electrolyte concentration of 0.1 mM. The significant impact of charged hydrogel functional groups to the impedance is damped at higher electrolyte concentration.

1 Introduction

Organic biosensors are promising devices for monitoring and detecting ions and small molecules at low concentrations in the body.[1] These devices are based on a class of materials, mixed ionic electronic conductors (MIECs), that conduct both ions and electrons and holes (electron vacancies).[2] Polymer MIECs are promising for biosensor applications due to their flexibility, biocompatibility, high ion and hole mobilities, and potential for functionalization.[3] The organic electrochemical transistor (OECT) is a device commonly applied to biological applications.[1,4] The OECT is comprised of a polymer semiconducting thin film between source and gain electrodes in contact with an electrolyte. A gate electrode immersed in the electrolyte completes the circuit.[5] Ions injected from the electrolyte into the semiconducting thin film displace electrons and holes, which then migrate and diffuse to the electrodes, driving an electronic current. The transistor design amplifies the electrical signal, resulting in a sensitive detection method for target ions.

Tang *et al.*[6] designed an OECT capable of detection of the neurotransmitter dopamine at the nanomolar level. An OECT designed by Bernards *et al.*[7] incorporated an enzyme, glucose oxidase, into the electrolyte to detect glucose concentration. *In vivo*, Khodagholy *et al.*[8,9] recorded local brain activity *via* an OECT at a spatial resolution and signal to noise ratio high enough to identify microseizures, a necessary step for epilepsy diagnosis. In this application, the OECT is directly in contact with the soft tissue of the brain. The OECT is bio-conformable due to the flexible nature of the semiconducting polymer used here, poly(3,4-ethylenedioxythiophene):polystyrene sulfonate (PEDOT:PSS). However, the PEDOT:PSS thin film is still much harder than the soft tissue, with a Young's modulus of ~2 GPa,[10,11] while the magnitude of the complex modulus for the soft grey matter in the brain is ~3 kPa.[12] This mechanical mismatch can lead to adverse effects caused by the strain induced by relative motion of the brain and the device.[13–16]

A hydrogel barrier between the soft tissue and the relatively hard device can be added to alleviate this mechanical strain. The hydrogel is designed to match the elastic modulus of the soft tissue while preserving electrical transport properties of the electrolyte such as conductivity and capacitance.[17] The hydrogel can be endowed with additional functionality, including device encapsulation to improve device lifetime and prevent loss of molecules necessary for sensing, such as enzymes for glucose sensing.[18,19]

The lifetime and performance of biosensors are significantly impacted by the "foreign body effect": the biosensors illicit an

Department of Chemical Engineering, Carnegie Mellon University, Pittsburgh, Pennsylvania, 15213, USA. E-mail: akhair@andrew.cmu.edu

immune response and the immune cells encapsulate the device in a collagen network.[20,21] Zwitterionic hydrogels such as poly(carboxybetaine methacrylate) (PCBMA) are ultra-low fouling: PCBMA was shown to resist the buildup of a collagen network for up to three months[21] and maintain device performance.[22] The functional groups on a zwitterionic polymer are acidic and basic. At the isoelectric point, the monomer is neutral: the negatively charged acidic group offsets the positive charge on the basic functional group. Below the isoelectric point, the monomer is positively charged: the basic functional group is positively charged and the acidic functional group is neutralized by the high hydrogen concentration in the electrolyte. Above the isoelectric point, the polymer is negatively charged. The isoelectric point pI is calculated from the dissociation constants for acidic and basic residues, K_a and K_b, respectively, as[23]

$$\mathrm{pI} = \frac{-\log K_a - \log K_b}{2}. \quad (1)$$

For use in biosensor applications, hydrogels must be electronically active to promote electronic and ionic charge transport.[24] Desirable electrical properties include high ion conductivity and low electrical impedance.[16] The electrical impedance Z is the ratio of the applied voltage to the current, and comprises both real (in phase with voltage) and imaginary (out of phase with voltage) contributions which are frequency dependent. The real part of impedance at low frequency is a measure of the electrical resistance of the fluid (inversely proportional to conductivity), while the imaginary part at low frequency relates to the capacitance of the double layer at the hydrogel–electrode interface. The frequency of neural electrical signals is 1 kHz,[25] so impedance is often measured at 1 kHz for biosensors designed for use in the skull.[3,24,26] Electrical impedance spectroscopy (EIS) is a valuable characterization tool for measuring capacitance and resistance. In addition, EIS can be applied to monitor the progress of processes such as gelation[27] and electroporation.[28] EIS is performed by applying a low amplitude, sinusoidal oscillation in the voltage between two electrodes of the form $\phi = -\frac{v}{2}\exp(i\omega t)$, where $i = \sqrt{-1}$, v is the voltage amplitude and ω is the angular frequency. The oscillating voltage is expressed here as a complex number where the real part of ϕ gives the physical applied voltage. At sufficiently low voltages the measured current is $I = I_m \exp(i\omega t)$, where I_m is a complex coefficient and the current oscillates at the same frequency as the applied voltage. The real part of I gives the physical current. Low voltage amplitude is defined as $v \ll k_B T/q$, where $v_T = k_B T/q \approx 25$ mV at $T = 300$ K is the thermal voltage, k_B is Boltzmann's constant, T is temperature, and q is the charge of a proton. In this linear regime, the current, ion concentration and potential in the hydrogel oscillate at the frequency of the applied potential, but can be out of phase.[29] The electrical impedance can be calculated from the oscillating applied potential and current as $Z = v\exp(i\omega t)/I_m \exp(i\omega t)$, where impedance Z is independent of time in the linear regime. The phase angle $\theta(\omega)$ between the applied potential and the measured current is defined as $\tan[\theta(\omega)] = \mathrm{Im}[Z(\omega)]/\mathrm{Re}[Z(\omega)]$. When the current is in phase with the applied potential, $\theta(\omega) = 0$, the system behaves as a resistor. Conversely, a system with a current completely out of phase with the applied potential $\theta(\omega) = \pi/2$ behaves as a capacitor. To determine the resistance and capacitance of the hydrogel and the diffusivity of the charge carriers, the current can be further analyzed by applying an equivalent circuit model.[30] These models are useful for interpreting EIS data, but limited in scope since they do not provide information about the micro-scale dynamics of the system, such as spatio-temporal ion densities.

The Poisson–Nernst–Planck (PNP) equations are partial, nonlinear differential equations that describe charge transport in electrochemical systems.[31,32] In the present work, the PNP equations are employed to model ion transport in zwitterionic hydrogels and to subsequently predict the current resulting from an oscillating applied potential and thence electrical impedance. At a pH not equal to the isoelectric point, the zwitterionic hydrogel carries a non-zero charge on the polymer backbone due to dissociation and association of the acidic and basic functional groups. The pH dependent charge density in the hydrogel will be incorporated into Poisson's equation relating charge density to the electric field.

Yates *et al.*[33] modeled an electrochemical cell with a four-step pH dependent surface reaction using the Gouy–Chapman–Stern model[34–36] for the electrical double layer, a region of counter-ion accumulation next to a charged surface. Bousse *et al.*[37] define an equivalent circuit model comprised of three elements. The double layer is modeled as a capacitor according to the Gouy–Chapman–Stern model, which is in parallel with the capacitance of adsorbed charge due to pH dependent surface reactions. The two capacitors are in series with a Warburg impedance, the impedance due to changes in the surface pH with the oscillating potential. Bousse *et al.*[38] apply this model to a field-effect transistor and derive an expression for the relation between pH, surface charge density, and the potential drop across the double layer. Landheer *et al.*[39] begin with this expression and the Poisson–Boltzmann equation to model the effect of pH on a field-effect transistor functionalized with biological macromolecules. *Via* an equivalent circuit model, Landheer *et al.*[39] calculate the capacitance of each component of the device and find that the biosensor sensitivity is highest at low electrolyte concentrations. In these previous works, the pH affected the reaction rate on the surface of the electrode, and was used to calculate the capacitance of the double layer.[38,39] In the case of a zwitterionic hydrogel, the pH changes the charge density throughout the cell and must be included in Poisson's equation relating the spatial variation in the electric field to the volumetric space charge density.

In Section 2, we propose a mathematical model for charge transport in zwitterionic hydrogels based on the PNP equations and equilibrium acid–base association relations. We then linearize the PNP equations for small applied voltages in Section 3 and solve for the electrical impedance. In Section 4 we apply an equivalent circuit model to the numerical solution of the PNP equations to calculate the conductivity, resistance, and capacitance of a model PCMBA hydrogel. We conclude in Section 5 with a possible extension of our model to account for

steric resistance due to hydrogel mesh spacing. In summary, our modeling framework enables the prediction of electrical transport properties of electrolyte-laden zwitterionic hydrogels, which is an important factor in the optimization of these materials for biosensor applications.

2 Mathematical model

Consider an electrolyte-laden zwitterionic hydrogel flanked by two planar, parallel, blocking electrodes (Fig. 1). The ion transport is mathematically described *via* the PNP equations, consisting of equations for the ion conservation and Poisson's equation. The zwitterionic hydrogel system requires four sets of ion conservation equations, one for each charged species: hydrogen ions, hydroxide ions, and dissociated cations and anions. The mean concentration of hydrogen and hydroxide depends on the pH of the electrolyte and the association and dissociation rate constants of the functional groups on the zwitterionic hydrogel backbone. The pH is determined by the composition of the electrolyte; for example, the pH of blood is pH = 7.4. The extent of dissociation of the acidic and basic functional groups depends directly on the pH according to the expressions for the acidic $[A^-]$ and basic $[HB^+]$ functional group concentrations developed below (8). We assume that the hydrogel is a thin film, with transport in the x direction and infinite dimensions in y and z compared to x (Fig. 1). The equations presented here are thus one-dimensional in x. The ion conservation equation is

$$\frac{\partial n_i}{\partial t} = \mu_i v_T \frac{\partial^2 n_i}{\partial x^2} + z_i \mu_i \frac{\partial}{\partial x}\left(n_i \frac{\partial \phi}{\partial x}\right), \tag{2}$$

where n_i is the ion concentration with the following naming convention for the subscript i: H = hydrogen, X = hydroxide, C = cation, and A = anion. Additional ionic species, *e.g.* for a multi-component electrolyte, could easily be incorporated by adding additional ion concentrations to (3) and solving (2) for each additional species. Time is t, x is position, $\mu_i = D_i/v_T$ is the ion mobility for each species, D_i is the diffusivity, and z_i is the valence of each ion. The diffusivity of ions in a hydrogel is closely coupled to the hydrogel mesh size.[40] This analysis is performed at the limit of a large mesh size compared to the hydrodynamic radius of the ions, hence the diffusivity is assumed to be the free solution value. The electric potential is ϕ. Poisson's equation is

$$\frac{\partial^2 \phi}{\partial x^2} = -\frac{q}{\varepsilon}\left(n_H - n_X + z_C n_C + z_A n_A + \rho_{gel}\right), \tag{3}$$

where ρ_{gel} is the charge density of the hydrogel and ε is the permittivity of the hydrogel. We do not account for local changes in permittivity with ion concentration due to ion-specific polarizability.[41] The charge on the hydrogel backbone is determined by the equilibrium reactions for the association and dissociation of hydrogen from the functional groups on the polymer backbone,

$$HA \rightleftarrows A^- + H^+, \text{ and } HB^+ \rightleftarrows B + H^+, \tag{4}$$

where A is the acidic functional group, B is the basic functional group, and H is hydrogen. The dissociation constants for these reactions are

$$K_a = \frac{[A^-]n_H}{[HA]}, \text{ and } K_b = \frac{[B]n_H}{[HB^+]}, \tag{5}$$

where [ ] indicates the concentration of the designated species. We assume that K_a and K_b are not functions of pH; see Section 4 for a discussion of the impact of this assumption on our calculations. We suppose that the reaction kinetics are fast in comparison to diffusion, thus the association–dissociation reactions are in equilibrium locally. At this limit, acid–base equilibrium expressions replace transport balances for neutral species.[42] We assume that the amount of water in the electrolyte is sufficiently large that the addition of relatively small amounts of hydrogen and hydroxide from the hydrogel acid–base reactions do not alter the water dissociation equilibrium. Hence, we do not consider water dissociation. The concentration of the charged functional groups A^- and HB^+ are calculated from an expression for the concentration of hydrogen ions as a function of pH and a mole balance for the total moles of monomers in the system. The pH is defined as

$$pH = -\log n_{H0}, \tag{6}$$

where n_{H0} is the uniform equilibrium ($v = 0$) hydrogen concentration. The mole balance on the total concentration of monomers N can be written for the acidic or basic functional groups as

$$N = [A^-] + [HA] = [HB^+] + [B]. \tag{7}$$

Eqn (5)–(7) can be rearranged to eliminate [HA] and [B], then solved for $[A^-]$ and $[HB^+]$, yielding

$$[A^-] = \frac{NK_a}{K_a + n_H}, \text{ and } [HB^+] = \frac{Nn_H}{K_b + n_H}. \tag{8}$$

If the pH is known, the equilibrium hydrogen concentration can be calculated according to (6). The concentration of charged functional groups is then given by (8), with the known values of the dissociation constants K_a and K_b, and the total concentration of monomer N. At low pH compared to the isoelectric point, pH < pI, the excess of hydrogen associates

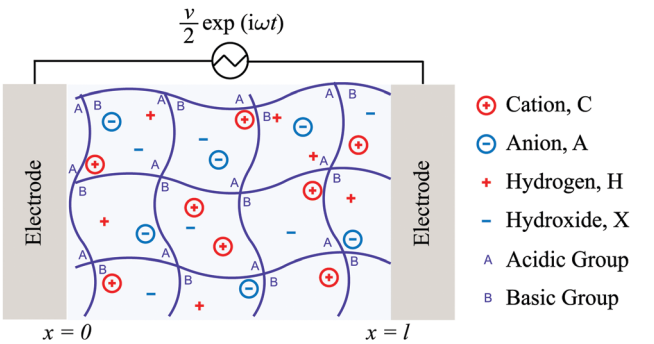

Fig. 1 Zwitterionic hydrogel sandwiched between two electrodes immersed in an electrolyte. The system contains two functional groups on the polymer backbone and four mobile ion species: cations, anions, hydrogen, and hydroxide. The current resulting from a low amplitude oscillating applied voltage $\frac{v}{2}\exp(i\omega t)$ is calculated.

with the acidic group, forming HA and reducing the concentration $[A^-]$. Similarly, the basic group accepts a hydrogen at low pH (4), forming HB^+. Thus, at low pH < pI, the hydrogel is positively charged. The converse is true at pH > pI. The charge density of the hydrogel is

$$\rho_{gel} = \frac{Nn_H}{K_b + n_H} - \frac{NK_a}{K_a + n_H}. \quad (9)$$

When pH = pI at the isoelectric point, the charge density of the hydrogel is $\rho_{gel} = 0$ according to (9). The equilibrium ion concentrations and potential at $v = 0$ are necessary to complete the model:

$$\text{At } v = 0, \phi(x) = 0, n_i(x) = n_{i0}, \text{ and } n_{C0} = -\frac{z_A}{z_C} n_{A0}, \quad (10)$$

where the expression for n_{A0} gives the anion concentration based on the cation concentration n_{C0} and the stoichiometry of the electrolyte. The appropriate boundary conditions for the ion concentrations are no flux at the electrodes in the absence of Faradaic reactions,

$$\frac{\partial n_i}{\partial x} = -z_i n_i \frac{\partial \phi}{\partial x} \text{ at } x = 0, l. \quad (11)$$

The applied potential at the electrodes oscillates in time according to

$$\phi(x = 0, t) = -\frac{v}{2} e^{i\omega t} \text{ and } \phi(x = l, t) = \frac{v}{2} e^{i\omega t}. \quad (12)$$

Thus the maximum total applied potential drop is v.

3 Linearized PNP equations

Electrical impedance spectroscopy is performed by measuring the time-varying current response to an AC voltage for a sweep in frequencies. The electrical impedance is then calculated from the ratio of the applied voltage to the measured current. This technique requires a linear current response, proportional to the applied voltage. In the nonlinear regime, the impedance is nonlinearly dependent on the amplitude of the applied voltage.[29,43] A linear current response is achieved by applying an applied voltage smaller than the thermal voltage in amplitude, $v \ll v_T \approx 25$ m.[30] In this regime, the PNP equations can be linearized by perturbing the ion concentration and potential in proportion to the small-amplitude oscillations in applied voltage. Thus the ion densities are expanded as

$$n_i = n_{i0} + n_{i1} e^{i\omega t}, \quad (13)$$

and the potential as

$$\phi = \phi_1 e^{i\omega t}. \quad (14)$$

where n_{i1} and ϕ_1 are $O(v)$. Note that the physical ion densities and potential are found by taking the real part of (13) and (14) after solving the linearized PNP equations. This is valid as we only consider linear departures from equilibrium. The leading order term $\phi_0 = 0$ in the absence of an equilibrium surface charge. When these expressions are inserted into (2) and (3), the resulting linearized charge conservation equation is

$$\frac{i\omega}{\mu_i} n_{i1} = v_T \frac{d^2 n_{i1}}{dx^2} + z_i n_{i0} \frac{d^2 \phi_1}{dx^2}. \quad (15)$$

The equilibrium terms for the ion density n_{i0} are constants, so they do not appear in the derivatives. Poisson's eqn (3) requires an additional step before linearization. The hydrogel charge density ρ_{gel} is not linearly dependent on the perturbed hydrogen concentration n_{H1}. We perform a regular expansion on (8) for $[A^-]$ and $[HB^+]$ in v to yield expressions that are valid for low amplitude voltages in comparison to the thermal voltage $k_B T/q$. The series expansion of (8) for the concentration of the dissociated acidic functional group is

$$[A^-] = \frac{NK_a}{K_a + (n_{H0} + n_{H1} e^{i\omega t})} \sim \frac{NK_a}{n_{H0} + K_a} - n_{H1} e^{i\omega t} \frac{NK_a}{(n_{H0} + K_a)^2}. \quad (16)$$

Similarly, the concentration of the dissociated basic functional group is

$$[HB^+] = \frac{N(n_{H0} + n_{H1} e^{i\omega t})}{K_b + (n_{H0} + n_{H1} e^{i\omega t})} \sim \frac{Nn_{H0}}{n_{H0} + K_b} + n_{H1} e^{i\omega t} \frac{NK_b}{(n_{H0} + K_b)^2}. \quad (17)$$

Expressions (16) and (17) are inserted into (9), which is combined with Poisson's eqn (3) to yield

$$\frac{\varepsilon}{q} e^{i\omega t} \frac{d^2 \phi_1}{dx^2} = -\left(\frac{Nn_{H0}}{n_{H0} + K_b} - \frac{NK_a}{n_{H0} + K_a} + n_{H0} - n_{X0} \right) - e^{i\omega t} \left(\frac{NK_b n_{H1}}{(n_{H0} + K_b)^2} + \frac{NK_a n_{H1}}{(n_{H0} + K_a)^2} + n_{H1} - n_{X1} + z_C n_{C1} + z_A n_{A1} \right). \quad (18)$$

The term independent of time in (18), the first term on the right-hand side, must be zero since it is voltage-independent. Hence,

$$0 = \frac{Nn_{H0}}{n_{i0} + K_b} - \frac{NK_a}{n_{i0} + K_a} + n_{H0} - n_{X0}. \quad (19)$$

Eqn (19) states that to maintain electroneutrality, in the absence of an applied field, the charge density on the hydrogel backbone is equal to the difference in concentration of the dissociated hydrogen and hydroxide in the electrolyte. The time-dependent equation for the perturbed potential ϕ_1 is then

$$-\frac{\varepsilon}{q} \frac{d^2 \phi_1}{dx^2} = \frac{NK_b n_{H1}}{(n_{H0} + K_b)^2} + \frac{NK_a n_{H1}}{(n_{H0} + K_a)^2} + n_{H1} - n_{X1} + z_C n_{C1} + z_A n_{A1}. \quad (20)$$

We can now solve eqn (15) and (20) together with the linearized form of the boundary conditions (11),

$$\frac{dn_{i1}}{dx} = -z_i n_{i0} \frac{d\phi_1}{dx} \text{ at } x = 0, l, \phi_1(0, t) = -v/2 \text{ and } \phi_1(l, t) = v/2, \quad (21)$$

to yield numerical solutions for the perturbed ion densities and applied potentials.

The electrical impedance is equal to the ratio of the voltage difference between the electrodes to the electrical current. The former equals $\Delta V = v \exp i\omega t$ in dimensional variables. The current $I(t)$ is equal to the derivative of the surface charge at the electrode, $I(t) = \mathrm{d}Q/\mathrm{d}t = \mathrm{d}(\varepsilon SE)/\mathrm{d}t$, S is the constant surface area of the electrode and $E = -\partial\phi/\partial x$ is the electric field.[29] Together with (14) this yields

$$Z = \frac{v \exp i\omega t}{\varepsilon S \frac{\partial^2}{\partial t \partial x}(\phi_1 \exp i\omega t)}. \quad (22)$$

After taking the mixed partial derivative, the expression for impedance Z is

$$Z = \frac{v}{\varepsilon S i\omega \left.\frac{\mathrm{d}\phi_1}{\mathrm{d}x}\right|_{x=0}}. \quad (23)$$

The impedance Z is a complex number, comprised of a real and imaginary part. The real part of impedance corresponds to the resistivity of the hydrogel and electrolyte, while the imaginary part is proportional to the inverse of the capacitance of the hydrogel and the double layers at the electrode–electrolyte interfaces at high and low frequency, respectively.

4 Impedance analysis

To calculate the electrical impedance at a sweep of frequencies, we solved eqn (15) and (20) along with the boundary conditions (21) for each of the four charged species (hydrogen, hydroxide, cations, and anions) with Matlab's bvp4c routine, a boundary value problem solver for ordinary differential equations based on collocation methods.[44] We then calculated the impedance according to (23). Since (15), (20), and (21) constitute a system of five linear ordinary differential equations, one could in principle pursue an analytical solution. However, the final expressions for the four ion concentration fields and electric potential would be lengthy and thus add little physical insight over a numerical solution.

At a pH unequal to the isoelectric point, the zwitterionic hydrogel carries a net charge. Fig. 2 is a Bode plot of the real and imaginary parts of impedance for a sweep of frequencies. The frequency range was selected to capture the crossover between the real and imaginary parts of impedance. The material parameters selected here, listed in Table 1, correspond to a model PCBMA hydrogel immersed in a symmetric binary electrolyte at a cation and anion concentrations of $n_{C0} = n_{A0} = 10^{-4}$ M and a monomer concentration of $N = 0.1$ M.[45] The cation diffusivity given is the diffusivity of sodium in water at infinite dilution.[31] The hydrogen diffusivity D_H given is for hydronium, H_3O^+, the hydrated form of the ion present in aqueous solution. This model electrolyte could be replaced with an asymmetric electrolyte by adjusting the ratio of the anion to cation mobility and the charge of each ion z_C and z_A. We choose a symmetric electrolyte to clearly show the impact of the hydrogel on electrical impedance. At the

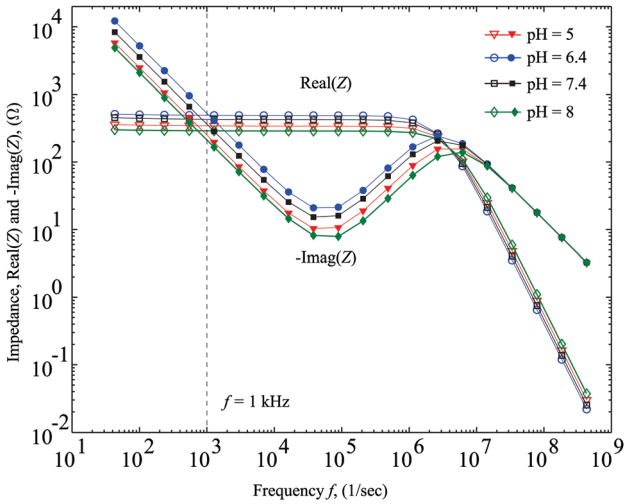

Fig. 2 The real (open symbols) and imaginary (filled symbols) parts of impedance are plotted for a range of frequencies and an equilibrium cation concentration of $n_{C0} = 10^{-4}$ M. Any deviation from the isoelectric point, pH = 6.4 results in a decrease in impedance. The dashed line indicates the physiological frequency of neural signals, 1 kHz. Lines through computed points are included to guide the eye.

isoelectric point of the PCBMA polymer, pI = 6.4, the impedance is larger for all frequencies than at pH = 5, 7.4, or 8. Deviations from the isoelectric point reduce both the real and imaginary portions of the electrical impedance due to the presence of a charge on the hydrogel backbone as well as an increase in the concentration of mobile hydrogen or hydroxide ions. The increase in the total number of charge carriers reduces the resistance of the hydrogel and increases the capacitance of electrical double layers at the electrode–electrolyte interface. The resistivity of the fluid corresponds to the real part of impedance at low frequencies,[46] which decreases in Fig. 2. The imaginary part of impedance at high frequency relates to the capacitance of the bulk fluid (a dielectric solvent), which is not dependent on the concentration of charge carriers. The double layer capacitance is inversely related to the limit of the imaginary part of impedance at low frequencies, so a decrease in $\mathrm{Im}(Z)$ as $f \to 0$ corresponds to an increase in the double layer capacitance, due to the increase in the concentration of charge carriers in the cell. These limits are discussed in more detail below. The physiological frequency of electrical signals in the brain, $f = 1$ kHz as indicated in Fig. 2, falls near the crossover between the real and imaginary parts of impedance, where both the resistance and double layer capacitance are significant. For biosensor encapsulation applications, a low impedance at $f = 1$ kHz is likely desirable to increase conductivity of ionic currents, which requires an electrolyte pH unequal to the isoelectric point.

Fig. 3 shows the cation and anion concentration profiles at pH = 6.4 and pH = 8 scaled by the ionic strength of the electrolyte $c_0 = (n_H + n_X + z_C^2 n_C + z_A^2 n_A)/2$. The cation and anion densities are antisymmetric around the midpoint of the cell, $x = l/2$. The anions and cations accumulate at the electrode ($x = 0$, l) interfaces forming electrical double layers. The capacitance of the double layer at pH = 8 is larger than at pH = 6.4.

Table 1 Material parameters for a model PCBMA hydrogel immersed in a symmetric binary electrolyte. These parameters were used in Fig. 2–8. In Fig. 5, the concentration is n_{C0} = 0.01, 0.1 and 1 M at a cell width $l = 10^{-6}$ m

Voltage v = 5 mV	Cation concentration $n_{C0} = 10^{-4}$ M	Cation charge $z_C = 1$
Anion charge $z_A = -1$	Hydrogel monomer concentration[45] N = 0.1 M	Surface area[45] $S = 10^{-4}$ m^2
Association constant[45] $K_a = 10^{-3}$ M	Dissociation constant[45] $K_b = 10^{-9.8}$ M	Diffusivity ratios D_i/D_C $\frac{D_H}{D_C} = \frac{D_X}{D_C} = 0.1, \frac{D_A}{D_C} = 1$
Hydrogel width[45] $l = 10^{-4}$ m	Relative permittivity of water ε_r = 80.4	Cation diffusivity[31] $D_C = 1.33 \times 10^{-9}$ m^2 s^{-1}

The charge on the hydrogel backbone at pH = 8 is immobile, whereas the mobile ions in the electrolyte are free to migrate and diffuse towards the electrode interfaces to screen the surface charge. The width of the electrical double layer is characterized by the Debye length $\lambda_D = \sqrt{\varepsilon k_B T/2q^2 c_0}$. The RC time, $\tau_{RC} = l\lambda_D/D$, is the characteristic timescale for double layer charging.[47] For the conditions in Fig. 2, the frequency of oscillations in the applied potential is equal to the rate of double layer charging at $f_{RC} = 1/\tau_{RC}$ = 430 Hz, which is the frequency corresponding to Re(Z) = Im(Z). At low frequencies $f < f_{RC}$, the double layer charges with ions. As frequency increases, ion migration and diffusion is slower than the fast oscillations in the polarity of the charged electrode, reducing the capacitance of the electrical double layer. In Fig. 2, the physiological frequency f = 1 kHz is higher than f_{RC} = 430 Hz, indicating that at this ion concentration, the double layer capacitance is reduced compared to the capacitance at $f < f_{RC}$.

The electric field in the double layer, shown in Fig. 4a scaled by v_T/l, is strongly dependent on the pH of the electrolyte. The magnitude of the electric field is much larger at pH = 8 than pH = 6.4 due to the increased charge density in the double layer (Fig. 3). The asymmetry around E = 0 results from changes in the polarity of the electrode potential at t = 4 ms depending on the frequency, where t = 4 ms is the time of first maximum in current at f = 43 Hz, an arbitrary selection. At large frequencies, the electric field is equal for both pH = 6.4 and 8 due to absence of an appreciable double layer formation; *i.e.* electroneutrality persists throughout the cell. In Fig. 4b, the hydrogel charge density scaled by the ionic strength of the electrolyte ρ_{gel}/c_0 is plotted against position x/l at pH = 8. The hydrogel charge density in the bulk is $\rho_{gel} = -15.5c_0$, while at pH = 6.4 we have ρ_{gel} = 0 (Fig. 4c). This significant hydrogel charge density accounts for the drop in electrical impedance from pH = 6.4 to pH = 8. Interestingly, the hydrogel charge density responds to the higher electric field (Fig. 4a) in the double layer, which is also reflected in the hydrogen and hydroxide concentrations. This results in a local change in the pH in the double layer compared to the bulk, indicating that even at pH = 6.4 we see local field-induced charging of the hydrogel.

The mean cation concentration in Fig. 2 is $n_{C0} = 10^{-4}$ M. However, in experiments the ion concentration in the electrolyte may be much higher, on the order of n_{C0} = 1 M.[45] In Fig. 5, the impedance curves are shown for mean concentrations of 1 M, 0.1 M, and 0.01 M at a physiological pH = 7.4 and cell width l = 1 μm.

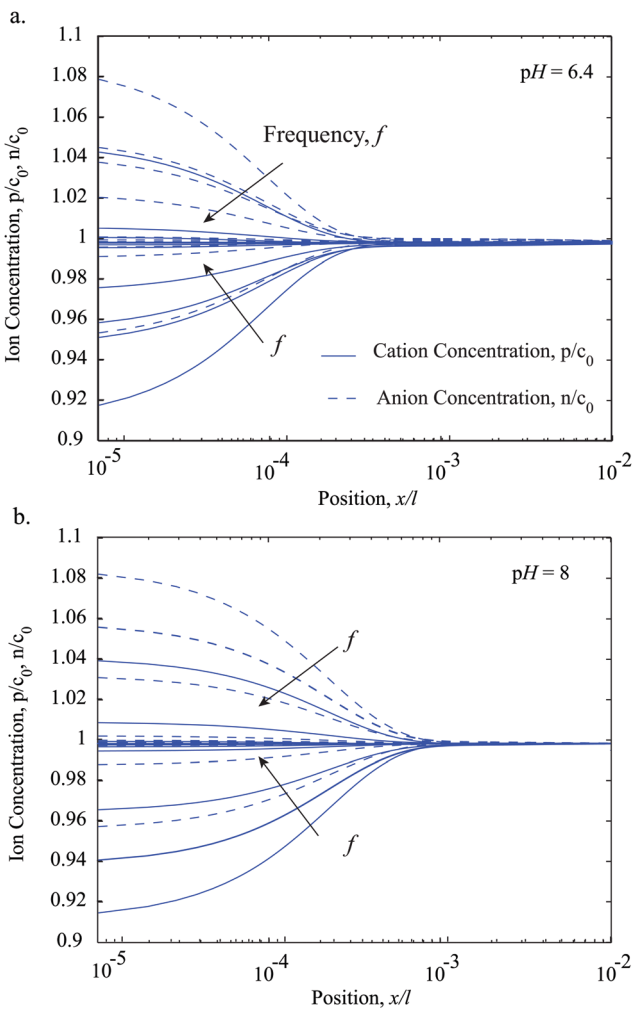

Fig. 3 The cation (solid line) and anion (dashed line) concentrations are shown for (a) pH = 6.4 and (b) pH = 8 at frequencies ranging from f = 43 to 4.3×10^8 Hz and an equilibrium cation concentration of $n_{C0} = 10^{-4}$ M. The ion concentration in the double layer increases as pH deviates from pH = 6.4. This is plotted for t = 4 ms, the time of the first peak in current at f = 43 Hz. The arrows indicated increasing frequency. At these pHs, $\lambda_D/l \sim O(10^{-4})$, beyond which the bulk is essentially uniform in concentration. Only one electrode is shown; the behavior is anti-symmetrical at the other electrode.

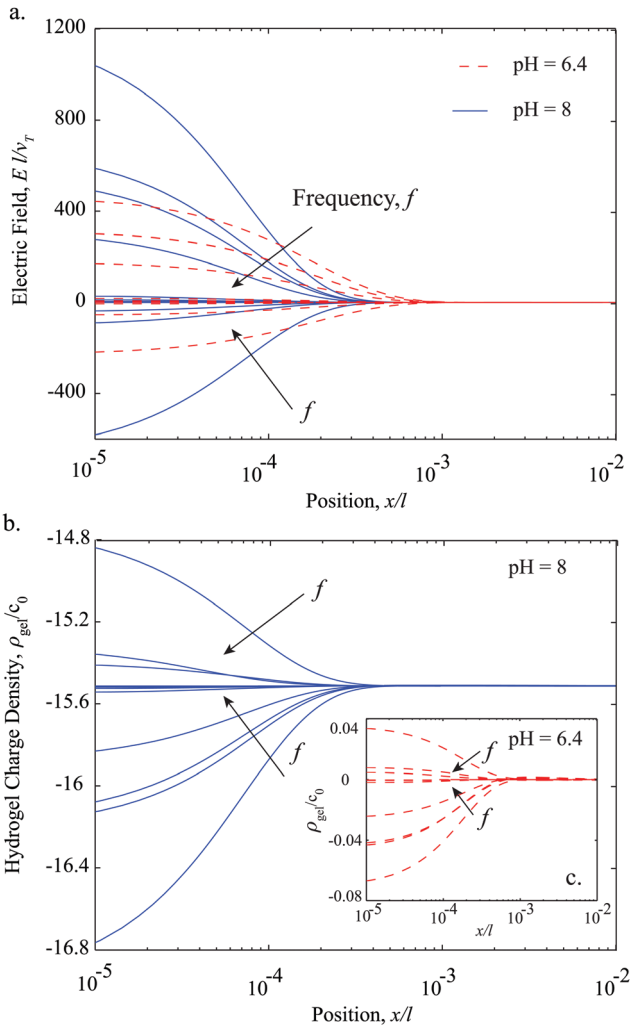

Fig. 4 (a) The electric field in the double layer at pH = 8 (line) is larger than the field at pH = 6.4 (dashed) due to the charge on the hydrogel backbone when the pH does not equal the isoelectric point. The hydrogel charge density scaled by the ionic strength of the electrolyte ρ_{gel}/c_0 for (b) pH = 8 and (c) pH = 6.4. In this figure, frequencies range from f = 43 to 4.3 × 10^8 Hz, the equilibrium cation concentration n_{C0} = 10^{-4} M, and time t = 4 ms.

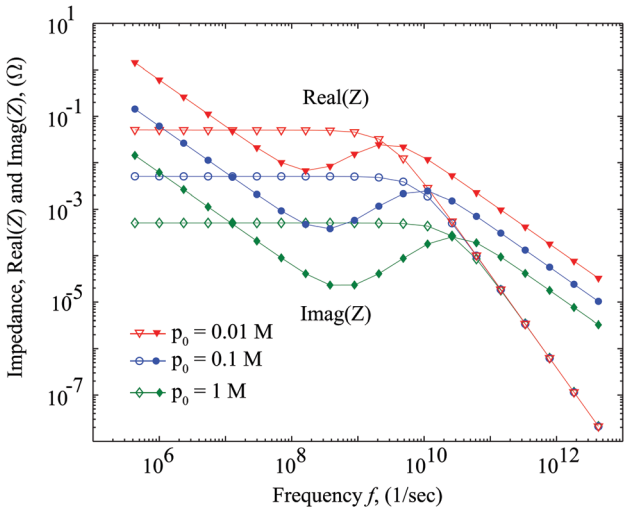

Fig. 5 The real (open symbols) and imaginary (filled symbols) parts of impedance are plotted for a range of frequencies for a cell of width l = 1 μm and pH = 7.4. The cation concentration varies from 10^{-2} M to 1 M. As the concentration increases, the impedance decreases at low frequencies.

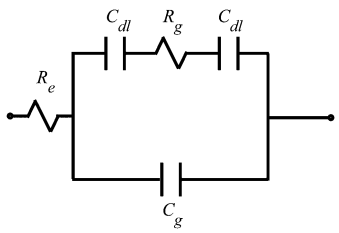

Fig. 6 Four-element circuit model consisting of the resistance of the external circuit R_e in series with the geometric capacitance of the cell C_g in parallel with the capacitance of each double layer C_{dl} and the resistance of the hydrogel R_g.

The narrower cell width was selected because the solution is numerically intractable at l = 10^{-4} m, due to rapid variation of the ion densities and electric field with the thin double layer. From the definition of the RC frequency f_{RC}, this change in cell width results in a shift in the impedance curves to larger frequency. We find that an order of magnitude increase in concentration decreases the real and imaginary parts of impedance by an order of magnitude at low frequency. This decrease stems from the addition of mobile ions to carry the current in the electrolyte, reducing the resistivity of the fluid. The imaginary part of impedance converges at a higher frequency than the frequency range plotted here.

The electrical impedance can be analyzed *via* a four element circuit model,[46] depicted in Fig. 6, consisting of the geometric capacitance of the cell C_g in parallel with the three elements in series: the resistance of the hydrogel R_g and the capacitance of the double layers C_{dl}. This unit is in series with the resistance of the external circuit, R_e, which is measurable in experiments at high frequency but not included in the PNP equation-based model presented in this work. The impedance derived for this four-element circuit model can be expressed as,[46]

$$Z = R_e + \left[\left(R_g + \frac{2i}{\omega C_{dl}}\right)^{-1} + \left(\frac{i}{\omega C_g}\right)^{-1}\right]^{-1}, \quad (24)$$

where ω = $2\pi f$ is the angular frequency. The real part of impedance is

$$\mathrm{Re}(Z) = R_e + \frac{R_g}{a + \omega^2 R_g^2 C_g^2}, \quad (25)$$

where a = 1 + 4c + 4c^2 and c = C_g/C_{dl}. The imaginary part of impedance is

$$\mathrm{Im}(Z) = R_g \frac{(2c + 4c^2)(\omega R_g C_g)^{-1} + \omega R_g C_g}{a + \omega^2 R_g^2 C_g^2}. \quad (26)$$

The asymptotic limits of these equations as $\omega \to 0$ and $\omega \to \infty$ can be used to calculate the resistances and capacitances. These asymptotic limits are depicted on a Bode plot[46] in Fig. 7 showing Re(Z) and ωIm(Z) plotted against frequency f

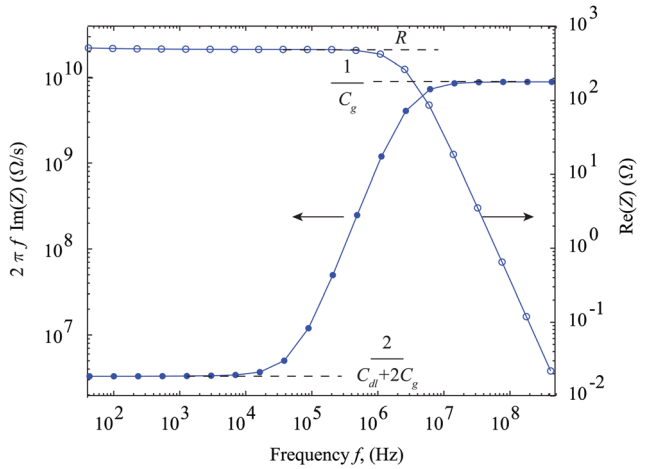

Fig. 7 The real (open circles) part of impedance Re(Z) and imaginary (filled circles) part of impedance multiplied by the angular frequency ωIm(Z) at pH = 6.4 and $n_{C0} = 10^{-4}$ M are plotted against frequency. The dashed lines indicate the asymptotic limits of (25) and (26).

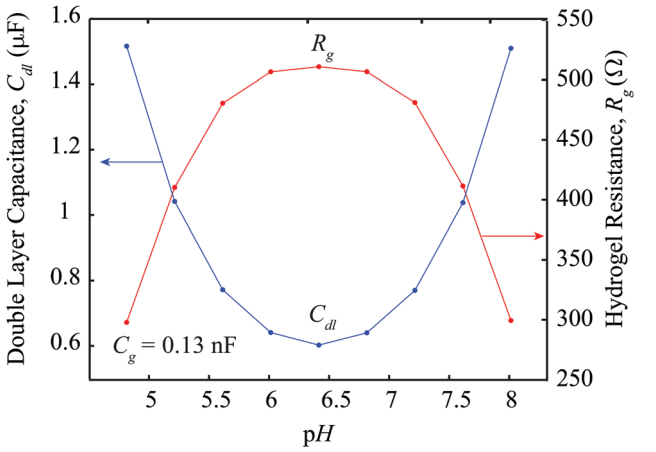

Fig. 8 The double layer capacitance C_{dl} and hydrogel resistance R_g are plotted as a function of pH. At the isoelectric point, C_{dl} is at a minimum and increases with deviations from the isoelectric point. R_g, conversely, decreases as pH deviates from the isoelectric point. The capacitance C_g is independent of pH.

at the isoelectric point pH = 6.4 and cation concentration $n_{C0} = 10^{-4}$ M, *i.e.* the data presented in Fig. 2. The asymptotic limits of (25) and (26) to leading order in ω as $\omega \to \infty$ are[46]

$$\lim_{\omega\to\infty} \mathrm{Re}(Z) = R_e + O(\omega^{-2}) \text{ and}$$
$$\lim_{\omega\to\infty} \omega\mathrm{Im}(Z) = \frac{1}{C_g} + O(\omega^{-2}). \quad (27)$$

The asymptotic limits as $\omega \to 0$ are

$$\lim_{\omega\to 0} \omega\mathrm{Im}(Z) = \frac{2}{C_{dl} + 2C_g} + O(\omega^2) \text{ and}$$
$$\lim_{\omega\to 0} \mathrm{Re}(Z) = \frac{R_g}{a} + O(\omega^2). \quad (28)$$

The resistances R_e and R_g and capacitances C_g and C_{dl} can be solved for by first calculating R_e and C_g from the limits of Re(Z) and ωIm(Z) as $\omega \to \infty$ according to (27). The limits as $\omega \to 0$ along with R_e, C_g, and the definitions of c and a yield the double layer capacitance C_{dl} and finally the hydrogel resistance R_g. We applied this method to the impedance spectrum at $n_{C0} = 10^{-4}$ and pH = 5, 6.4, 7.4, 8 (Fig. 2) to calculate the resistances and capacitances in Fig. 8.

The resistance R_g decreases as the pH deviates from pH = 6.4 due to an increase in the total concentration of mobile charge in the cell, including dissociated salt and hydroxide and hydrogen ions. The capacitance of the double layers increases, as shown in Fig. 3, with the concentration of charge carriers, and is four orders of magnitude larger than the geometric capacitance of the cell C_g, which is independent of charge carrier concentration. The calculated capacitance C_g in Fig. 5 is C_g = 13.3 nF. $C_g \sim 1/L$,[46] so the change in the width of the cell from $L = 10^{-4}$ m to $L = 10^{-6}$ m is responsible for the two order of magnitude increase in C_g compared to the capacitance C_g = 0.133 nF in Fig. 8.

The effect of pH on impedance is significant when the electrolyte ion concentration is $n_{C0} = 10^{-4}$ M. However, at higher concentrations the increase in the total concentration of mobile ions due to a change in pH is minimal. At n_{C0} = 1 M, the impedance decrease is $O(10^{-9}\ \Omega)$ as the pH increases from pH = 6.4 to pH = 7.4. The impact of the charge on the hydrogel backbone on impedance is limited to low ion concentration for this model PCBMA hydrogel. The effect of pH would be more pronounced for a zwitterionic hydrogel with divalent or trivalent functional groups due to the increase in charge per functional group from $z = \pm 1$ to $z = \pm 2$ or 3 when completely dissociated. Our model can be readily adapted to analyze multi-valent functional groups. The presence of such groups can enhance counter-ion condensation due to strong electrostatic attraction with charge on the hydrogel backbone, thereby reducing the effective charge number of the hydrogel.[48] This reduction would increase impedance relative to our calculations, due to a diminishment in the mobile charge arising from acid–base association–dissociation reactions. A first order model for this effect would be to utilize a 'renormalized' monomer concentration, $\tilde{N}$ say, that is much less than the 'bare' concentration N. Relaxation of our assumption that K_a and K_b do not vary with pH would also lead to an increase in impedance. For instance, at pH > pI the dissociation of HA into A^- and H^- will be suppressed due to electrostatic attraction of protons with the negatively charged polyelectrolyte backbone. This effect could be modeled using a modified Henderson–Hasselbalch equation.[49] The result of this suppression is a reduction in the amount of mobile charge originating from the hydrogel and hence an increase in impedance. Therefore, the hydrogel resistance R_g and double layer capacitance C_{dl} would increase and decrease, respectively, due to the two above-mentioned effects. Nonetheless, R_g and C_{dl} would still attain maximum and minimum values, respectively, at the isoelectric point. Finally, we assumed that the volume of hydrogel is constant upon changing pH, despite the variation in osmotic pressure with the degree of dissociation of

acid/base groups. That is, we suppose that the hydrogel is flanked by rigid electrodes and not free to expand or contract on changing pH. This would induce a mechanical stress on the electrodes; hence, a full analysis of the effect of hyrdogel volume change should incorporate this mechanical effect, in addition to the change in acid/base group spatial distribution due to volume change. We anticipate that this effect would be damped at higher electrolyte concentration as osmotic pressure variation with pH would be small compared to the large osmotic pressure due to the high concentration of cations and anions.

5 Conclusions

We have developed a mathematical model for ion transport in zwitterionic hydrogels based on the PNP equations and equilibrium equations for acid–base association and dissociation. This model incorporates the effect of pH on the charge of the functional groups on the hydrogel backbone by adding a term for the charge density of the hydrogel to Poisson's eqn (3). The PNP equations were linearized for low-amplitude oscillations in the applied voltage and solved numerically. The electrical impedance was calculated according to (23). The predicted impedance curves at a sweep of frequencies were analyzed *via* a four-element circuit model to extract parameters including resistivity, double layer capacitance, and the geometric capacitance to characterize the expected electrical properties of an electrolyte–hydrogel system. We have shown that the impedance decreases as the pH deviates from the pH at the isoelectric point of PCBMA hydrogel, pH = 6.4. The decrease in resistance of the hydrogel and increase in the double layer capacitance at the electrode–hydrogel interface are due to an increase in the concentration of mobile ions in the hydrogel and charged functional groups on the zwitterionic hydrogel backbone. At high electrolyte ion concentrations, we find that the total charge on the hydrogel backbone is small in comparison to the total salt concentration, thus the impedance does not change significantly with pH at those concentrations.

Our model can guide the design of hydrogels for biosensor encapsulation applications. For example, the zwitterionic hydrogel will not give anomalous electrical measurements in systems with high salt concentration, since the electrolyte ion concentration dominates the impedance. However, if the electrical signal is weak, a hydrogel with a large charge density on the polymer backbone compared to the ionic strength of the electrolyte may aid in device performance due to reduced electrical impedance and increased conductivity of the electrical signal.

The charge transport model presented in this paper is modular in nature; the boundary conditions, equilibrium conditions, and parameters can be altered to include additional physics. For example, to account for spatial variation in the mesh size of the hydrogel, the total concentration of the hydrogel N can be replaced with a function of position x. This change does not impact the analysis because the PNP equations are linearized with respect to time, not position. If the mesh size of the hydrogel is on the order of the hydrodynamic radius of the ion, the ion mobility is impeded. The ion mobility μ_i can be adjusted by a Brinkman factor[50] to account for the reduction in mobility. However, the incorporation of such additional physical effects could make the interpretation of the resulting impedance spectrum in terms of an equivalent circuit challenging, since there is not a one-to-one mapping between an equivalent circuit and impedance spectrum.[51,52]

The hydrogel here is sandwiched between two electrodes, as per the typical electrical impedance spectroscopy setup. For use as a mechanical barrier for biosensors, the hydrogel is in contact with soft tissue and a polymer-coated electrode.[21,24] The method presented to incorporate acid–base dissociation into the PNP equations can be applied to hydrogel encapsulated biosensors by altering the boundary conditions to allow for time-dependent ion concentration at the soft tissue-hydrogel interface and ion injection from the hydrogel into the polymer film driven by an applied potential. For example, in Feicht *et al.*,[53] we modeled ionic and electronic charge transport in a polymer coated electrode *via* the PNP equations. The hydrogel and polymer charge transport models are compatible and could be incorporated into a device-level model for a zwitterionic hydrogel-encapsulated organic biosensor.

Acknowledgements

We gratefully acknowledge Professor Christopher Bettinger for introducing us to this topic and for useful discussions. S. E. F. acknowledges support by the National Science Foundation Graduate Research Fellowship under Grant No. 0946825. We also acknowledge National Science Foundation CAREER support under CBET-1350647.

References

1 J. Leger, *Adv. Mater.*, 2008, **20**, 837–841.
2 I. Riess, *Solid State Ionics*, 2003, **157**, 1–17.
3 M. Berggren and A. Richter-Dahlfors, *Adv. Mater.*, 2007, **19**, 3201–3213.
4 T. Cramer, A. Campana, F. Leonardi, S. Casalini, A. Kyndiah, M. Murgia and F. Biscarini, *J. Mater. Chem. B*, 2013, **1**, 3728–3741.
5 G. P. Kittlesen, H. S. White and M. S. Wrighton, *J. Am. Chem. Soc.*, 1984, **106**, 7389–7396.
6 H. Tang, P. Lin, H. L. Chan and F. Yan, *Biosens. Bioelectron.*, 2011, **26**, 4559–4563.
7 D. Bernards, D. Macaya, M. Nikolou, J. DeFranco, S. Takamatsu and G. Malliaras, *J. Mater. Chem.*, 2007, **18**, 116–120.
8 D. Khodagholy, T. Doublet, P. Quilichini, M. Gurfinkel, P. Leleux, A. Ghestem, E. Ismailova, T. Hervé, S. Sanaur, C. Bernard and G. G. Malliaras, *Nat. Commun.*, 2013, **4**, 1575.
9 D. Khodagholy, J. Rivnay, M. Sessolo, M. Gurfinkel, P. Leleux, L. H. Jimison, E. Stavrinidou, T. Herve, S. Sanaur, R. M. Owens and G. G. Malliaras, *Nat. Commun.*, 2013, **4**, 2133.

10 U. Lang, N. Naujoks and J. Dual, *Synth. Met.*, 2009, **159**, 473–479.
11 D. Tahk, H. H. Lee and D.-Y. Khang, *Macromolecules*, 2009, **42**, 7079–7083.
12 M. A. Green, L. E. Bilston and R. Sinkus, *NMR Biomed.*, 2008, **21**, 755–764.
13 D. E. Discher, P. Janmey and Y.-l. Wang, *Science*, 2005, **310**, 1139–1143.
14 H. Lee, R. V. Bellamkonda, W. Sun and M. E. Levenston, *Journal of Neural Engineering*, 2005, **2**, 81.
15 J. Subbaroyan, D. C. Martin and D. R. Kipke, *Journal of Neural Engineering*, 2005, **2**, 103.
16 L. Rao, H. Zhou, T. Li, C. Li and Y. Y. Duan, *Acta Biomater.*, 2012, **8**, 2233–2242.
17 D. Seliktar, *Science*, 2012, **336**, 1124–1128.
18 C. P. Quinn, C. P. Pathak, A. Heller and J. A. Hubbell, *Biomaterials*, 1995, **16**, 389–396.
19 R. J. Russell, M. V. Pishko, C. C. Gefrides, M. J. McShane and G. L. Cote, *Anal. Chem.*, 1999, **71**, 3126–3132.
20 B. D. Ratner, *J. Controlled Release*, 2002, **78**, 211–218.
21 L. Zhang, Z. Cao, T. Bai, L. Carr, J.-R. Ella-Menye, C. Irvin, B. D. Ratner and S. Jiang, *Nat. Biotechnol.*, 2013, **31**, 553–556.
22 W. Yang, H. Xue, L. R. Carr, J. Wang and S. Jiang, *Biosens. Bioelectron.*, 2011, **26**, 2454–2459.
23 A. B. Lowe and C. L. McCormick, *Chem. Rev.*, 2002, **102**, 4177–4190.
24 H. Ding, M. Zhong, Y. J. Kim, P. Pholpabu, A. Balasubramanian, C. M. Hui, H. He, H. Yang, K. Matyjaszewski and C. J. Bettinger, *ACS Nano*, 2014, **8**, 4348–4357.
25 Y. Xiao, D. C. Martin, X. Cui and M. Shenai, *Appl. Biochem. Biotechnol.*, 2006, **128**, 117–129.
26 N. A. Kotov, J. O. Winter, I. P. Clements, E. Jan, B. P. Timko, S. Campidelli, S. Pathak, A. Mazzatenta, C. M. Lieber and M. Prato, *et al.*, *Adv. Mater.*, 2009, **21**, 3970–4004.
27 A. Martin, J. Wojciechowski, H. Warren, M. in het Panhuis and P. Thordarson, *Soft Matter*, 2016, **12**, 2700–2707.
28 A. Suri, R. Campos, D. Rackus, N. Spiller, C. Richardson, L.-O. Pålsson and R. Kataky, *Soft Matter*, 2011, **7**, 7071–7077.
29 F. Freire, G. Barbero and M. Scalerandi, *Phys. Rev. E: Stat., Nonlinear, Soft Matter Phys.*, 2006, **73**, 051202.
30 E. Barsoukov and J. R. Macdonald, *Impedance spectroscopy: theory, experiment, and applications*, John Wiley & Sons, 2005.
31 J. Newman and K. E. Thomas-Alyea, *Electrochemical systems*, John Wiley & Sons, 2012.
32 J. Ross MacDonald and D. Franceschetti, *J. Chem. Phys.*, 1978, **68**, 1614–1636.
33 D. E. Yates, S. Levine and T. W. Healy, *J. Chem. Soc., Faraday Trans. 1*, 1974, **70**, 1807–1818.
34 G. Gouy, *J. Phys.*, 1910, **9**, 457–468.
35 D. L. Chapman, *London, Edinburgh Dublin Philos. Mag. J. Sci.*, 1913, **25**, 475–481.
36 O. Stern, *Z. Elektrochem.*, 1924, **30**, 1014–1020.
37 L. Bousse and P. Bergveld, *J. Electroanal. Chem. Interfacial Electrochem.*, 1983, **152**, 25–39.
38 L. Bousse, N. F. De Rooij and P. Bergveld, *IEEE Trans. Electron Devices*, 1983, **30**, 1263–1270.
39 D. Landheer, G. Aers, W. McKinnon, M. Deen and J. Ranuarez, *J. Appl. Phys.*, 2005, **98**, 044701.
40 S. Zustiak, H. Boukari and J. Leach, *Soft Matter*, 2010, **6**, 3609–3618.
41 M. Hatlo, R. Van Roij and L. Lue, *EPL*, 2012, **97**, 28010.
42 J. Baygents and D. Saville, *J. Colloid Interface Sci.*, 1991, **146**, 9–37.
43 R. Stout and A. Khair, *Phys. Rev. E: Stat., Nonlinear, Soft Matter Phys.*, 2015, **92**, 032305.
44 L. Shampine, I. Gladwell and S. Thompson, *Solving ODEs with MATLAB*, Cambridge University Press, 2003.
45 C. Bettinger, private communication, 8/5/2014.
46 B. A. Yezer, A. S. Khair, P. J. Sides and D. C. Prieve, *J. Colloid Interface Sci.*, 2015, **449**, 2–12.
47 M. Z. Bazant, K. Thornton and A. Ajdari, *Phys. Rev. E: Stat., Nonlinear, Soft Matter Phys.*, 2004, **70**, 021506.
48 S. Alexander, P. Chakin, P. Grant, G. Morales, P. Pincus and D. Hone, *J. Chem. Phys.*, 1984, **80**, 5776–5781.
49 J. Koetz and S. Kosmella, *Polyelectrolytes and Nanoparticles*, Springer, 2007.
50 H. Brinkman, *Appl. Sci. Res.*, 1949, **1**, 27–34.
51 D. Franceschetti and J. Ross MacDonald, *J. Electroanal. Chem.*, 1977, **82**, 271–301.
52 J. Ross MacDonald, *Ann. Biomed. Eng.*, 1992, **20**, 289–305.
53 S. E. Feicht, G. D. Degen and A. S. Khair, *AIChE J.*, 2015, **61**, 1447–1454.

